Optimization and stability boundaries for the synchronization of semiconductor lasers with external optical feedback

Y. Chembo Kouomou[1,2] and P. Woafo[1,*]

[1]*Laboratoire de Mécanique, Faculté des Sciences, Université de Yaoundé I, Boîte Postal 812, Yaoundé, Cameroon*
[2]*Division of Telecommunication Technical Studies, Minpostel, Yaoundé, Cameroon*

We perform a stability and optimization analysis for the synchronization of unidirectionally coupled external-cavity semiconductor lasers. Using rigorous stability criteria, we qualitatively derive the boundaries of the high-quality synchronization basin. The underlying influence of Hopf bifurcations on the stability of the synchronization manifold is also investigated.

I. INTRODUCTION

Synchronization of chaotic systems has been the focus of intense research activities in recent years [1–3]. This paradoxical phenomenon was soon considered as an interesting candidate to ensure secure telecommunications [4–6]. Effectively, one can encode an information-bearing signal into the output of a chaotic transmitter, while a synchronous receiver identifies the masking chaotic component, which is then extracted to reveal the original transmitted message. Since nowadays telecommunication networks require large-capacity information transmission and ultrafast processing, semiconductor lasers have become indispensable and widespread devices, precisely as optoelectronic emitter-receiver systems. That is why the chaotic synchronization of semiconductor lasers (laser diodes) has currently gathered so much attention [4,7–9].

Chaos can be generated in laser diodes through external optical feedback (EOF). Indeed, for weak EOF, improved frequency stability, linewidth narrowing, and noise reduction have been noticed. But as the feedback increases, the infinite dimensionality created by the feedback delay can induce a drastic spectral broadening, which is sometimes referred to as coherence collapse [10–15]. The coherence collapse state is associated with hyperchaotic attractors whose complexity is expected to provide high-level security for the encoded messages, even at the subnanosecond time scale. As far as potential applications to telecommunications are concerned, quite interesting realizations have been set up. For example, Goedgebuer and co-workers have built a robust cryptosystem based on the synchronization of tunable laser diodes with wavelength hyperchaos [16], and while using an open-loop chaotic synchronization scheme, Fisher *et al.* have successfully encoded and decoded signals at a frequency up to 1 GHz [17].

Despite these important experimental and theoretical results, many crucial questions still require particular attention, mainly about the stability and optimization of synchronization processes. The stability of synchronization can be understood in two distinct ways. From the first point of view, stability implies indefinite boundedness for the drive and response variables. Within that scheme, synchronization is unstable only when the coupling provokes a sustained growth to infinity for the state master and/or slave variables. This kind of instability is quite grave, because it can cause irreversible damage to the coupled drive-response system. It has been demonstrated that its underlying mechanism is generally the parametric resonance induced by the overly dominant frequencies of the Fourier spectrum corresponding to the master oscillator [18,19]. From the second point of view, stability implies robustness, and in that sense, the synchronization is unstable when it is subjected to intermittent desynchronization events, i.e., when the figurative phase point is burst-likely repelled from the synchronization manifold. This bubbling phenomenon is explained by the fact that some unstable invariant sets for which the largest transverse sub-Lyapunov exponent is positive can be embedded within an attractor even when the largest transverse sub-Lyapunov exponent for the attractor as a whole is negative [20–22]. It is important to notice that for the application of external-cavity semiconductor laser (ECSL) synchronization to secure telecommunications, these bursts would have catastrophic consequences, because during the desynchronization intervals, the encoded information cannot be recovered and is therefore irreversibly lost. Throughout all the paper, we will hence always refer to this second stability definition, because it is more constraining as it includes the first one.

The key issue of this paper is to derive for unidirectionally coupled ECSL's an analytic approximation for the boundaries of the synchronization basin, both in the regular and chaotic regimes. We therefore aim to establish rigorous stability constraints able to guarantee high-quality synchronization.

The paper is organized as follows. In Sec. II, we present the rate equations corresponding to our coupling scheme, and the stability analysis of the synchronized laser diodes is performed in Sec. III. The last section is devoted to the conclusion. The iterative integration of all ordinary differential equations is performed with the fourth-order Runge-Kutta algorithm, while all the nonlinear algebraic equations will be solved through the Newton-Raphson algorithm.

---

*Corresponding author. Electronic address:
pwoafo@uycdc.uninet.cm

TABLE I. Parameter values used for the numerical simulations (based on Al_xGaAs_{1-x} semiconductor lasers [8]).

Symbol	Parameter	Value
g	Gain coefficient	8.4×10^{-13} m^3 s^{-1}
α	Linewidth enhancement factor	3
r_0	Facet amplitude reflectivity	0.556
N_{th}	Carrier density at threshold	2.018×10^{24} m^{-3}
J	Injection current density	$1.3J_{th}$
τ_s	Carrier lifetime	2.04 ns
τ_p	Photon lifetime	1.927 ps
τ_{in}	Round-trip time in the laser cavity	8 ps
λ	Wavelength	800.0 nm

II. MODEL OF UNIDIRECTIONALLY COUPLED EXTERNAL-CAVITY SEMICONDUCTOR LASERS

The nonlinear dynamics of ECSL's can be modelized through the Lang-Kobayashi rate equations [23]. This model is quite accurate in the single-longitudinal-mode regime when the optical feedback is weak to moderate. The significant variables are the carrier density N and the complex electric field defined by its amplitude $\hat{E}$ and its slowly varying phase ϕ. In dimensionless units, the Lang-Kobayashi equations read

$$\dot{E} = nE + \gamma E_\tau \cos(\omega\tau + \phi - \phi_\tau),$$

$$\dot{\phi} = \alpha n - \gamma\left(\frac{E_\tau}{E}\right)\sin(\omega\tau + \phi - \phi_\tau),$$

$$\dot{n} = \varepsilon[p - n - (1+2n)E^2], \tag{1a}$$

with the following rescalings:

$$\varepsilon = \tau_p/\tau_s, \quad p = \frac{1}{2}gN_{th}\tau_p\left(\frac{J}{J_{th}} - 1\right),$$

$$\gamma = \tau_p\left(\frac{1-r_0^2}{\tau_{in}r_0}\right)r_{ext}, \quad K = \tau_p\left(\frac{1-r_0^2}{\tau_{in}r_0}\right)k_{cp},$$

$$\tau = T/\tau_p, \quad \tau_c = T_c/\tau_p, \quad \omega = \frac{2\pi c}{\lambda}\tau_p, \tag{1b}$$

and

$$E = \left(\frac{1}{2}g\tau_s\right)^{1/2}\hat{E},$$

$$n = \frac{1}{2}gN_{th}\tau_p\left(\frac{N}{N_{th}} - 1\right). \tag{1c}$$

Table I presents the meaning and numerical values of the laser diode characteristics. In Eq. (1a), the overdot denotes the derivative relatively to the reduced time t/τ_p and the subscripts denote delayed variables: i.e., we assume that if V is a variable (E, ϕ, or n) and θ the delay, $V_\theta \equiv V(t-\theta)$. The first delay to appear in our equations is the dimensionless

round-trip delay $\tau = T/\tau_p$, where $T = 2L_{ext}/c$ and L_{ext} is the length of the external cavity [8]. The optical feedback is taken into account through the coefficient γ, which is proportional to the external reflectivity percentage r_{ext}. p stands for the injection current density, whose influence upon the ECSL dynamics is extremely decisive for the large-scale structure of the laser's oscillations. Effectively, when p is very close to the threshold value $p_{th} = 0$, the ECSL enters into what is usually called the low-frequency fluctuation (LFF) regime [12,15]. In our case, p is much greater, so that the chaotic oscillations have a relatively constant mean value which is $\sqrt{p} \cong 0.7$, corresponding to the trivial steady-state regime.

Theoretically, two fundamentally different types of chaotic synchronization can occur for ECSL's depending on the strengths of both the feedback and the coupling [9]. For the first type, which is referred to as conventional synchronization, the slave variables synchronize (up to a constant for some of them) with those of the master at time $t - T_c$, where T_c is the coupling delay, i.e., the time required for the command signal emitted by the master to reach the slave. Here we will rather use a technique belonging to the second group and which is based on the continuous chaos control scheme proposed by Pyragas [24].

According to Murakami and Ohtsubo, the synchronization of identical ECSL's can be achieved with an unidirectional coupling scheme provided that some physical constraints are fulfilled (see details in Ref. [8]). Using appropriate external mirrors, the master laser diode injects into the active region of the slave laser diode a fraction of its electromagnetic output, which thereby plays the role of a command signal. An optical isolator guarantees the unidirectionality of the coupling. The slave ECSL is subjected to a second optical feedback, which completes a retroactive control loop. The slave system equations corresponding to that particular coupling are

$$\dot{\tilde{E}} = \tilde{n}\tilde{E} + \gamma\tilde{E}_\tau\cos(\omega\tau + \tilde{\phi} - \tilde{\phi}_\tau) + K[E_{\tau_c}\cos(\omega\tau_c + \tilde{\phi} - \phi_{\tau_c})$$
$$- \tilde{E}_\tau\cos(\omega\tau + \tilde{\phi} - \tilde{\phi}_\tau)],$$

$$\dot{\tilde{\phi}} = \alpha\tilde{n} - \gamma\left(\frac{\tilde{E}_\tau}{\tilde{E}}\right)\sin(\omega\tau + \tilde{\phi} - \tilde{\phi}_\tau) - K\left[\left(\frac{E_{\tau_c}}{\tilde{E}}\right)\sin(\omega\tau_c + \tilde{\phi}\right.$$
$$- \phi_{\tau_c}) - \left(\frac{\tilde{E}_\tau}{\tilde{E}}\right)\sin(\omega\tau + \tilde{\phi} - \tilde{\phi}_\tau)\bigg],$$

$$\dot{n} = \varepsilon[p - \tilde{n} - (1+2\tilde{n})\tilde{E}^2], \tag{2}$$

where the tilde indicates the slave variables and K accounts for the optical coupling. Note that the coefficient K is proportional to the coupling efficiency percentage k_{cp}. A second delay also appears in our equations, which is the coupling delay $\tau_c = T_c/\tau_p$. Thus Eqs. (2) are double-delay differential equations (DDDE's), as τ and τ_c simultaneously influence the ECSL dynamics [25]. If we had considered multiple reflections with the external reflectors, additional delays would

have been introduced, leading to increasingly complicated equations. Anyway, these additional delays are not relevant here since the optical feedback is weak. DDDE's in synchronization theory seem to be very promising. Effectively, assuming that the synchronization manifold is $V(t-\tau_c)=\widetilde{V}(t-\tau)$, they enable us to achieve anticipated, instantaneous, or delayed synchronization depending on the fact that τ_c can be smaller, equal, or greater than τ. Throughout all the paper, we will focus for the sake of exemplification on instantaneous synchronization, and therefore we will only deal with a single degenerated delay ($\tau \equiv \tau_c$). This particular case may seem to be restrictive, but it can nevertheless give a deep insight into what occurs for the general double-delay model.

III. STABILITY BOUNDARIES OF THE SYNCHRONIZATION BASIN

As we have earlier noticed, quasiperfect synchronization is required for most of its potential applications. Consequently, the determination of necessary and sufficient conditions for high-quality synchronization currently constitutes an important field of investigations [18–20,22]. For synchronized ECSL's, the stability is often performed through the linear stability analysis of the external-cavity modes (ECM's) [7,8]. Unfortunately, this approach rapidly loses its validity for typically nonlinear states (multiperiodic, quasiperiodic, and chaotic). Moreover, it does not provide a general stability constraint or limits for the synchronization basin.

It was first believed that stable synchronization could be ensured by the negativity of the so-called transverse sub-Lyapunov exponents [1]. However, this condition has further been proved to be necessary, but not sufficient, because these exponents describe the chaotic attractor as a whole, whereas stability also depends on localized invariant sets embedded within this attractor. It has also been suggested that uniformly negative instantaneous eigenvalues could be an interesting alternative. Unfortunately, this "ubiquitous local stability" criteria is exclusively relevant for the long-term behavior and fails to make a statement about the stability of the transient motion, as the continuously changing eigenvalues and eigenvectors can induce parametric resonance [18,19]. Later, sufficient stability conditions either derived from Lyapunov functions or from anamorphosis-based methods were proposed. Anyway, these latter techniques do not generally apply when the coupling is inextricably nonlinear (and delayed) as in our case.

On the other hand, Brown and Rulkov have proposed an original approach which enables one to derive rigorous stability criteria, i.e., sufficient constraints which guarantee high-quality (burst-free) synchronization between identical systems with drive-response coupling [26]. Moreover, their method can precisely be used to design the efficient couplings. Effectively, the Brown-Rulkov (BR) technique leads to explicit analytic stability conditions and therefore offers a judicious guidance for the choice of the suitable system parameters. We aim to use this method to derive the stability boundaries of the synchronization basin.

Let us consider the master and slave vector fields as

$$\mathbf{x}=(E,\phi,n),$$

$$\widetilde{\mathbf{x}}=(\widetilde{E},\widetilde{\phi},\widetilde{n}). \tag{3}$$

Our evolution equations (1a) and (2) may now be written in vectorial notation as

$$\dot{\mathbf{x}}=\mathbf{F}(\mathbf{x},\mathbf{x}_\tau),$$

$$\dot{\widetilde{\mathbf{x}}}=\mathbf{F}(\widetilde{\mathbf{x}},\widetilde{\mathbf{x}}_\tau)+\mathbf{C}(\widetilde{\mathbf{x}},\widetilde{\mathbf{x}}_\tau,\mathbf{x}_\tau), \tag{4}$$

where $\mathbf{F}$ represents the uncoupled ECSL and $\mathbf{C}$ the unidirectional coupling. If we define the coordinate transverse to the synchronization manifold,

$$\mathbf{w}=\widetilde{\mathbf{x}}-\mathbf{x}, \tag{5}$$

as the deviation vector between the drive and response subsystems, it obeys

$$\dot{\mathbf{w}}=\left[\frac{\partial[\mathbf{F}(\widetilde{\mathbf{x}},\widetilde{\mathbf{x}}_\tau)+\mathbf{C}(\widetilde{\mathbf{x}},\widetilde{\mathbf{x}}_\tau,\mathbf{x}_\tau)]}{\partial\widetilde{\mathbf{x}}}\right]_{\mathbf{w}=0}\mathbf{w}$$

$$+\left[\frac{\partial[\mathbf{F}(\widetilde{\mathbf{x}},\widetilde{\mathbf{x}}_\tau)+\mathbf{C}(\widetilde{\mathbf{x}},\widetilde{\mathbf{x}}_\tau,\mathbf{x}_\tau)]}{\partial\widetilde{\mathbf{x}}_\tau}\right]_{\mathbf{w}_\tau=0}\mathbf{w}_\tau \tag{6}$$

at a linear approximation. Explicitly developing the Jacobian matrices yields

$$\dot{\mathbf{w}}=[\mathbf{H}(\mathbf{x},\mathbf{x}_\tau)]\mathbf{w}+(\gamma-K)[\mathbf{G}(\mathbf{x},\mathbf{x}_\tau)]\mathbf{w}_\tau, \tag{7}$$

where

$$\mathbf{H}(\mathbf{x},\mathbf{x}_\tau)$$

$$=\begin{bmatrix} n & -\gamma E_\tau\sin\varphi & E \\ \gamma\dfrac{E_\tau}{E^2}\sin\varphi & -\gamma\dfrac{E_\tau}{E}\cos\varphi & \alpha \\ -2\varepsilon(1+2n)E & 0 & -\varepsilon(1+2E^2) \end{bmatrix} \tag{8}$$

and

$$\mathbf{G}(\mathbf{x},\mathbf{x}_\tau)=\begin{bmatrix} \cos\varphi & E_\tau\sin\varphi & 0 \\ -\dfrac{1}{E}\sin\varphi & \dfrac{E_\tau}{E}\cos\varphi & 0 \\ 0 & 0 & 0 \end{bmatrix}. \tag{9}$$

We have introduced $\varphi=\omega\tau+\phi-\phi_\tau$ as the phase delay. We now decompose the $\mathbf{H}$ matrix into its time average and variable components according to

$$\mathbf{H}(\mathbf{x},\mathbf{x}_\tau)=\mathbf{A}+\mathbf{B}(t), \tag{10}$$

with

$$\mathbf{A}=\langle\mathbf{H}(\mathbf{x},\mathbf{x}_\tau)\rangle,$$

$$\mathbf{B}(t)=\mathbf{H}(\mathbf{x},\mathbf{x}_\tau)-\langle\mathbf{H}(\mathbf{x},\mathbf{x}_\tau)\rangle. \tag{11}$$

Here $\langle\cdot\rangle$ denotes the time average along the driving trajectory. In first approximation, the matrix $\mathbf{B}$ can be considered

as proportional to γ. This approximation becomes more accurate as p increases, since in that case E oscillates around the $\sqrt{p}$ mean value [15]. Hence $\mathbf{H}$ can finally be expressed as

$$\mathbf{H}(\mathbf{x}, \mathbf{x}_\tau) = \mathbf{A} + \gamma \mathbf{Q}(t). \tag{12}$$

We emphasize that $\mathbf{Q}$ still weakly depends on γ anyway. The $\mathbf{A}$ matrix can be diagonalized to $\mathbf{D}$ through the transfer matrix $\mathbf{P}$. Therefore the vector $\mathbf{z}$, which is the $\mathbf{w}$ counterpart in the $\mathbf{D}$ basis, satisfies

$$\mathbf{z}(t) = [\mathbf{U}(t, t_0)] \mathbf{z}(t_0) + \int_{t_0}^t \gamma \mathbf{U}(t, s) [\mathbf{P}^{-1} \mathbf{Q}(s) \mathbf{P}] \mathbf{z}(s) ds$$

$$+ \int_{t_0}^t (\gamma - K) \mathbf{U}(t, s) [\mathbf{P}^{-1} \mathbf{G}(s) \mathbf{P}] \mathbf{z}_\tau(s) ds, \tag{13}$$

where $\mathbf{U}(t, t_0) = \exp[\mathbf{D}(t - t_0)]$ is the exponential operator. Linearly stable synchronized behavior is expected if $\|\mathbf{z}(t)\| \to 0$ as $t \to +\infty$. This convergence to 0 can occur if and only if each of the three blocks in Eq. (13) individually vanishes at long term.

Let us consider Λ_1, Λ_2, and Λ_3, the eigenvalues of $\mathbf{A}$, ordered as $\mathrm{Re}[\Lambda_1] \geq \mathrm{Re}[\Lambda_2] \geq \mathrm{Re}[\Lambda_3]$, where $\mathrm{Re}[\Lambda]$ is the real part of Λ. The first block of Eq. (13) converges to $\mathbf{0}$ if

$$-\mathrm{Re}[\Lambda_1] > 0. \tag{14}$$

It is our first stability requirement. This condition is reminiscent of the negativity of transverse sub-Lyapunov exponents, but in fact, Eq. (14) is more constraining, because sub-Lyapunov exponents are obtained through the $\mathbf{H}$ and $\mathbf{G}$ matrices, while Λ_1 is derived through $\mathbf{A}$, which is only the time-average component of $\mathbf{H}$.

The second block uniformly tends to $\mathbf{0}$ if the exponential operator imposes onto the $\mathbf{P}^{-1} \mathbf{Q} \mathbf{P}$ term its decay behavior. One can use norms to convert Eq. (13) into an inequality and, therefore, uniform convergence is ensured if

$$-\mathrm{Re}[\Lambda_1] > |\gamma| \langle \|\mathbf{P}^{-1} \mathbf{Q} \mathbf{P}\| \rangle, \tag{15}$$

that is,

$$\gamma < \frac{-\mathrm{Re}[\Lambda_1]}{\langle \|\mathbf{P}^{-1} \mathbf{Q} \mathbf{P}\| \rangle}. \tag{16}$$

It appears that the feedback coefficient has an upper limit which depends on the system's parameters. We stress again that the right-hand side of inequality (16) depends on γ, so that this inequality is mathematically implicit.

At last, the third block of Eq. (13) converges to zero if

$$-\mathrm{Re}[\Lambda_1] > |\gamma - K| \langle \|\mathbf{P}^{-1} \mathbf{G} \mathbf{P}\| \rangle \tag{17}$$

or, more explicitly,

$$\gamma - \left(\frac{-\mathrm{Re}[\Lambda_1]}{\langle \|\mathbf{P}^{-1} \mathbf{G} \mathbf{P}\| \rangle} \right) < K < \gamma + \left(\frac{-\mathrm{Re}[\Lambda_1]}{\langle \|\mathbf{P}^{-1} \mathbf{G} \mathbf{P}\| \rangle} \right). \tag{18}$$

This latter relation means that the stability basin lies within a band around the central value $K = \gamma$.

To summarize, the BR technique has provided three stability constraints, which are Eqs. (14), (16), and (18). We will further see that the numerical simulation qualitatively confirms these analytic statements.

For this numerical comparison, two radically opposite situations will be considered: the stable and unstable bifurcation states. To understand the reason for this differentiation, one should recall the bifurcation behavior of ECSL's [8]. Their nonlinear dynamics is strongly determined by the interplay between the relaxation oscillation frequency of the solitary semiconductor laser $[f_R = \sqrt{g(J - J_{\mathrm{th}})}/2\pi = \Omega_R/2\pi]$ and the external-cavity-mode spacing frequency ($f_{\mathrm{ext}} = 1/T = c/2L_{\mathrm{ext}}$). As the feedback coefficient γ increases, the initially stable eigenmodes undergo a first Hopf bifurcation (first HB) to periodic oscillations. It is demonstrated [13,14,27] that when $\Omega_R T$ is an odd multiple of π, the competition between f_R and f_{ext} is the weakest possible and, hence, the critical Hopf bifurcation value is very low: it is a stable bifurcation. On the other hand, when $\Omega_R T$ is an even multiple of π, this competition is the strongest possible, and the critical Hopf bifurcation value is quite high: it is here an unstable bifurcation. When γ is further increased, the interval of periodic oscillations is followed in both cases by a two-frequency quasiperiodic regime after a second Hopf bifurcation (second HB). This bifurcation sequence is universal for ECSL's, even though the critical bifurcation values are different for each eigenmode [11]. For all related numerical simulations, we have taken $L_{\mathrm{ext}} = 15$ cm for the stable bifurcation and $L_{\mathrm{ext}} = 12$ cm for the unstable one, so that we have found the Hopf bifurcation values couple of r_{ext} to be, respectively, (0.34, 0.89) for the stable bifurcation regime and (1.04, 1.54) for the unstable case (in units of %). These Hopf bifurcations are indicated in Figs. 1 and 2 by vertical solid lines.

To check for the validity of our analytic approach, one should represent the numerical synchronization basin in the r_{ext}-k_{cp} figurative plane. This has already been done in [8], and the synchronization basins that have been obtained qualitatively fit with our predictions, both in the stable and unstable bifurcation cases. Effectively, a maximal r_{ext} value is observed, as well as the band shape around the maximal stability diagonal, $r_{\mathrm{ext}} = k_{cp}$. We remind the reader that γ and K are, respectively, proportional to r_{ext} and k_{cp} [see Eq. (1b)].

The stability is mostly affected along the diagonal: therefore, we introduce a new variable

$$q_d = \sqrt{\frac{r_{\mathrm{ext}}^2 + k_{cp}^2}{2}}, \tag{19}$$

which is the curvilinear coordinate along the diagonal segment $r_{\mathrm{ext}} = k_{cp}$. Hence, since q_d is *always* simultaneously equal to r_{ext} and k_{cp}, varying q_d implies varying the feedback rate γ and the coupling rate K at the same time. In Figs. 1(a) and 2(a), we have plotted $\mathrm{Re}[\Lambda_1]$ as a function of q_d. It appears that for the stable bifurcation, the BR technique foresees synchronization for very weak q_d. As q_d increases, $\mathrm{Re}[\Lambda_1]$ becomes positive and intermittently drops below 0 for $q_d > 1.79$. Nevertheless, synchronization cannot be re-
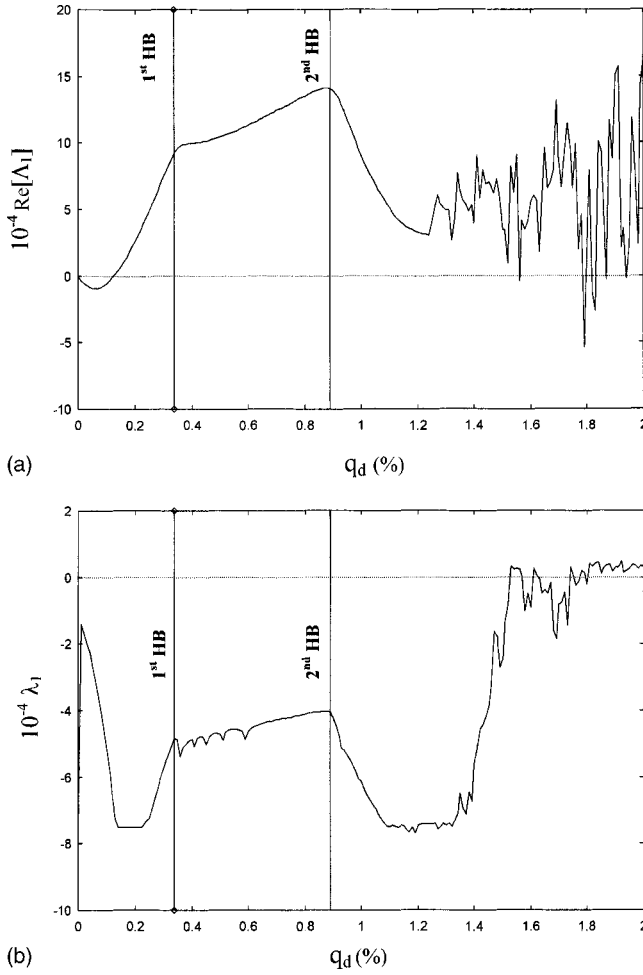
FIG. 1. Stable bifurcation case. (a) Variations of Re[Λ_1] and (b) variations of λ_1 along the diagonal $r_{\text{ext}} = k_{cp}$.

FIG. 2. Unstable bifurcation case. (a) Variations of Re[Λ_1] and (b) variations of λ_1 along the diagonal $r_{\text{ext}} = k_{cp}$.

gained in that case because the second stability requirement is no longer respected: q_d (here corresponding to γ) is then too large and ($-$Re[Λ_1]) too low to satisfy the inequality (16). For the unstable bifurcation, synchronization for very weak feedback is also guaranteed. Globally, the BR technique leads to interesting results as it can, however, enable us to understand the geometrical form of the synchronization basin in the r_{ext}-k_{cp} figurative plane. Unfortunately, it is striking that the consequent stability criteria are overly strong. For example, they fail to foresee stability within the chaotic range, which is, however, the most interesting.

Nevertheless, we can circumvent this deficiency by diagonalizing **H** with its related sub-Lyapunov exponents $\lambda_1 \geq \lambda_2 \geq \lambda_3$, rather than **A** with the Re[Λ] eigenvalues in the BR method. The resulting stability criteria thereby lose their mathematical rigor, but—and this is the most important—they still provide necessary conditions for the stable synchronization to occur. Proceeding in that way, the three stability criteria (14), (16), and (18) degenerate into two, which are

$$-\lambda_1 > 0 \qquad (20)$$

and
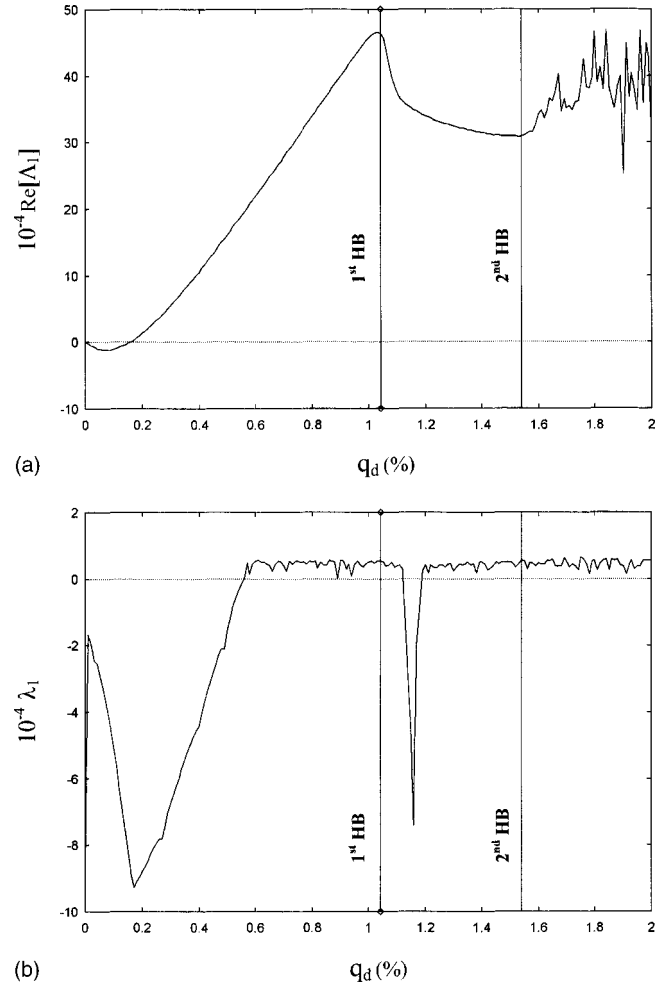
$$\gamma - \left(\frac{-\lambda_1}{\langle \|\mathbf{L}^{-1}\mathbf{GL}\| \rangle} \right) < K < \gamma + \left(\frac{-\lambda_1}{\langle \|\mathbf{L}^{-1}\mathbf{GL}\| \rangle} \right), \qquad (21)$$

where **L** is the transfer matrix from **H** to its diagonal counterpart. Equation (20) replaces both Eqs. (14) and (16), and then intrinsically contains the upper limitation of γ. Moreover, it exactly corresponds to the well-known standard stability condition. On the other hand, Eq. (21) stands for Eq. (18) with the same geometrical meaning.

Figures 1(b) and 2(b) display the variations of λ_1 as a function of q_d, and it clearly appears that the new set of stability criteria (20) and (21) more accurately fits with the numerical boundaries of the synchronization basin. Equation (20) decides the stability of the synchronization along the diagonal, while Eq. (21) does the same for the transverse direction. Effectively, it appears that as q_d is increased (along the diagonal), the synchronization is stable when λ_1 is negative, while in the perpendicular direction, the width of the basin varies accordingly to $|\lambda_1|$; i.e., the basin is larger as $|\lambda_1|$ is greater. Therefore, one can conclude (even though it is not new) that the synchronization is optimized when λ_1 is the most negative possible. Nevertheless, we recall that Eqs. (20) and (21) are not rigorous.

Although it does not appear explicitly, Hopf bifurcations can dangerously threaten the stability of synchronization [6,8,25]. Effectively, when we carefully examine Figs. 1(b) and 2(b), we note that $|\lambda_1|$ drastically drops to 0 around the bifurcation values. For the stable bifurcation, these drops do not reach the positive upper half-plane. But for the unstable case, the first and second HB's succeed in destabilizing the synchronization along the diagonal. Since within the chaotic regime the bifurcation sequence subsists under a fractal form, chaotic synchronization can be lost because of a slight variation of a relevant bifurcation parameter. Fortunately, these undesirable HB's can analytically be localized in the periodic regime for ECSL's, thus indicating in the first approximation the parameter ranges to avoid in priority [13,14,27].

This may be particularly important for the synchronization of ECSL's in the presence of parameter mismatch (or noise). Effectively, it is known that the maximal synchronization error $\|w\|_{max}$ is roughly proportional to the global mismatch (or to the intensity of the noise), but inversely proportional to the average largest sub-Lyapunov exponent λ_1 around the hyperchaotic attractor. Even though this reasoning is not mathematically rigorous, it can serve as an interesting guideline for the choice of the coupling parameters. Since the suitable parameters should preferably induce the lowest sub-Lyapunov exponents, the HB's should degrade the tolerance to parameter mismatch (noise). The numerical simulations we have performed confirm this argumentation,

and they show that the synchronization error inversely follows the variations of $|\lambda_1|$, i.e., drastically increases near the HB's. Therefore, one can expect that control and anticontrol of these Hopf bifurcations will soon play a key role for the optimization of synchronization in both the periodic and chaotic states [28].

IV. CONCLUSION

In this paper, we have performed the stability and optimization analysis for the synchronization of unidirectionally coupled external-cavity semiconductor lasers, both in their (multi)periodic and hyperchaotic regimes. The Brown-Rulkov technique has provided stability constraints which have enabled us to foresee the shape of the synchronization basin. The underlying influence of Hopf bifurcations has been highlighted. We have noticed that they can even destabilize the synchronization manifold in the most unfavorable cases.

A logic continuation of this work could be the stability analysis of the most general delay configuration, i.e., the nondegenerated double-delay system. Even though several numerical studies have been performed for $\tau \neq \tau_c$ [7–9], almost nothing has been done to investigate analytically how the interplay between the two delays τ and τ_c influences the shape of the synchronization basin. At last, further studies can also be devoted to extend this analytic approach to other types of ECSL couplings.

[1] L. M. Pecora and T. L. Carroll, Phys. Rev. Lett. **64**, 821 (1990).

[2] N. F. Rulkov, M. M. Sushchik, L. S. Tsimring, and H. D. I. Abarbanel, Phys. Rev. E **51**, 980 (1995).

[3] L. Kocarev and U. Parlitz, Phys. Rev. Lett. **76**, 1816 (1996).

[4] C. R. Mirasso, P. Colet, and P. Garcia-Fernandez, IEEE Photonics Technol. Lett. **8**, 299 (1996).

[5] N. J. Corron and D. W. Hahs, IEEE Trans. Circuits Syst., I: Fundam. Theory Appl. **44**, 373 (1997).

[6] P. Woafo, Phys. Lett. A **267**, 31 (2000).

[7] V. Ahlers, U. Parlitz, and W. Lauterborn, Phys. Rev. E **58**, 7208 (1998).

[8] A. Murakami and J. Ohtsubo, Phys. Rev. E **63**, 066203 (2001).

[9] A. Locquet, F. Rogister, M. Sciamanna, P. Mégret, and M. Blondel, Phys. Rev. E **64**, 045203 (2001).

[10] J. Sacher, W. Elsässer, and E. O. Göbel, Phys. Rev. Lett. **63**, 2224 (1989).

[11] C. Masoller, Phys. Rev. A **50**, 2569 (1994).

[12] T. Sano, Phys. Rev. A **50**, 2719 (1994).

[13] A. M. Levine, G. H. M. v. Tartwijk, D. Lenstra, and T. Erneux, Phys. Rev. A **52**, R3436 (1995).

[14] C. Masoller and N. B. Abraham, Phys. Rev. A **57**, 1313 (1998).

[15] T. Heil, I. Fisher, and W. Elsässer, Phys. Rev. A **58**, R2672

(1998).

[16] J.-P. Goedgebuer, L. Larger, and H. Porte, Phys. Rev. Lett. **80**, 2249 (1998).

[17] I. Fisher, Y. Liu, and P. Davis, Phys. Rev. A **62**, 011801 (2000).

[18] N. J. Corron, Phys. Rev. E **63**, 055203 (2001).

[19] Y. Chembo Kouomou and P. Woafo, Phys. Lett. A **298**, 18 (2002).

[20] P. Ashwin, J. Buescu, and I. Stewart, Phys. Lett. A **193**, 126 (1994).

[21] J. F. Heagy, T. L. Carroll, and L. M. Pecora, Phys. Rev. E **52**, R1253 (1995).

[22] D. J. Gauthier and J. C. Bienfang, Phys. Rev. Lett. **77**, 1751 (1996).

[23] R. Lang and K. Kobayashi, IEEE J. Quantum Electron. **16**, 347 (1980).

[24] K. Pyragas, Phys. Lett. A **181**, 203 (1993); Y. Chembo Kouomou and P. Woafo, Phys. Rev. E **66**, 036205 (2002).

[25] C. Marriott, R. Vallée, and C. Delisle, Phys. Rev. A **40**, 3420 (1989).

[26] R. Brown and N. F. Rulkov, Phys. Rev. Lett. **78**, 4189 (1997).

[27] A. Ritter and H. Haug, J. Opt. Soc. Am. B **10**, 130 (1993).

[28] D. S. Chen, H. O. Wang, and G. Chen, IEEE Trans. Circuits Syst., I: Fundam. Theory Appl. **48**, 661 (2001).